Laboratory Study on Diffusion and Migration of Grout in Rock Mass Fracture Network

Bin Liu[1]; Haomin Sang[2]; Quansheng Liu[3]; He Liu[4]; Yucong Pan[5]; and Yongshui Kang[6]

Abstract: The flow process of grout in a rock mass fracture network is an important part to judge the effect of grouting in engineering. Till date, little research has been done on the diffusion and migration pattern of grout in a random fracture network. Based on this, herein, a visualized fracture grouting test system with constant pressure was developed, consisting of pressure supply equipment, constant-pressure pulping equipment, fracture simulation equipment, and monitoring equipment. The system can simulate the flow process of the fracture network under the effect of various parameters such as the grouting pressure, grout characteristics, and fracture aperture and achieve the real-time monitoring of grout pressure, flow velocity, and diffusion distance in a random fracture network. Also, the governing equation of grout flow in a single rough fracture was obtained. The reliability of the test system was proved by the comparison of the single fracture grouting theory with the test results. Moreover, the grouting diffusion mechanism of the random fracture network was studied. The results show that (1) the pressure at the same point in the fracture increased with an increase in the grouting pressure and a decrease in the fracture aperture and was not affected by a change in the grout viscosity. (2) After the grout was dispersed into several branches in the fracture network, the pressures dropped significantly, the flow velocity decreased, and the pressure of each branch and flow distribution coefficient were greatly affected by the angle of bifurcation (intersection) fracture. The development of a test system and study results has a certain guiding value for grouting engineering. **DOI: 10.1061/(ASCE)GM.1943-5622.0001901**.

Author keywords: Grouting; Fracture network; Diffusion and migration; Simulation test.

Introduction

During the excavation and unloading process, several joints and fractures are generated inside the rock mass. Unstable failure may occur in severe cases, which affects the surrounding rock stability and engineering safety (Kang et al. 2014, 2018). Grouting is one of the important means to repair the fractured rock mass and improve the surrounding rock strength. The diffusion range of the grout in a fractured rock mass is an important measure for evaluating the grouting effect. The methods to study the pattern of grouting diffusion primarily include theoretical research, laboratory testing, numerical simulation, and a field test. The researchers have developed multiple theoretical formulas for the grout flow in a single fracture and obtained several important conclusions (Baker 1974; Hässler et al. 1992; Chen et al. 2004; Xiao et al. 2017). However, the engineering geological conditions and grouting process are oversimplified in theoretical research and numerical simulations, causing a difference between the research results and actual engineering. It is difficult to visually observe the grout flow in the fracture in a field test, and the relevant parameters cannot be obtained. Compared to the aforementioned methods, the laboratory test can realistically simulate the grouting process and the relevant test parameters can be obtained. Several other research works have focused on this method (Zhang et al. 2011; Minto et al. 2016).

In recent decades, both domestic and foreign scholars have obtained a series of results for the grouting simulation tests. The test space has also transformed from one dimensional to two dimensional and three dimensional to maximize the reduction of field grouting conditions of the project and to achieve a wider range of the grouting laws. Funehag and Thörn (2018) employed acrylic glass to fabricate two fracture channels with the fracture apertures of 125 and 200 μm, respectively. They also performed a simulation test of grout diffusion in the radial fractures by assuming cement grout as a Bingham fluid to verify the correctness of grout diffusion and migration theory in a single fracture. Owing to a short time in this test, the physical and chemical changes of the grout were ignored. The maximum penetration length of the grout in the fractures was obtained through the test, which has a positive guiding significance in practical engineering. Ding et al. (2019) employed an advanced integrated apparatus to simulate the synchronous grouting process in a quasi-rectangular shield tunnel. By using different grouting cases, the quasi-rectangular tunnel was obtained as the best grouting method. By installing the soil pressure gauges and cameras at the inside of the organic glass segment, the grouting

[1]Associate Professor, State Key Laboratory of Geomechanics and Geotechnical Engineering, Institute of Rock and Soil Mechanics, Chinese Academy of Sciences, Wuhan 430071, Hubei, China.

[2]Ph.D. Candidate, State Key Laboratory of Geomechanics and Geotechnical Engineering, Institute of Rock and Soil Mechanics, Chinese Academy of Sciences, Wuhan 430071, Hubei, China; Univ. of Chinese Academy of Sciences, Beijing 100049, China.

[3]Professor, Key Laboratory of Safety for Geotechnical and Structural Engineering of Hubei Province, School of Civil Engineering, Wuhan Univ., Wuhan 430072, Hubei, China.

[4]Ph.D. Candidate, State Key Laboratory of Geomechanics and Geotechnical Engineering, Institute of Rock and Soil Mechanics, Chinese Academy of Sciences, Wuhan 430071, Hubei, China; Univ. of Chinese Academy of Sciences, Beijing 100049, China.

[5]Associate Professor, Key Laboratory of Safety for Geotechnical and Structural Engineering of Hubei Province, School of Civil Engineering, Wuhan Univ., Wuhan 430072, Hubei, China.

[6]Associate Professor, State Key Laboratory of Geomechanics and Geotechnical Engineering, Institute of Rock and Soil Mechanics, Chinese Academy of Sciences, Wuhan 430071, Hubei, China (corresponding author). Email: yskang@whrsm.ac.cn

Note. This manuscript was submitted on January 15, 2020; approved on September 3, 2020; published online on November 7, 2020. Discussion period open until April 7, 2021; separate discussions must be submitted for individual papers. This paper is part of the ***International Journal of Geomechanics***, © ASCE, ISSN 1532-3641.

pressure, the grouting flow path, and grouting pressure distribution were measured and analyzed. Zhang et al. (2016) developed a visual large-scale three-dimensional fracture grouting test system with flowing water. This test achieved the grouting simulation with flowing water under low and high pressures. The flow velocity sensors were set up to establish an information acquisition system of flow velocity, pressure, and temperature. Simulation tests of the grout diffusion and cementation and reinforcement under the condition of flowing water were successfully performed, and the fractured grouting theory with flowing water was established in line with the engineering practice.

The grouting laboratory testing focuses on the grout flow process in a single fracture, and there have been a few studies on the grout flow in complex and fracture networks. Therefore, considering the shortcomings, herein, a rock mass grouting system has been independently developed. Under the constant pressure grouting conditions, the grout pressure, diffusion distance, and diffusion time of the grout flowing in the rough fracture network were monitored and analyzed, and the relevant patterns were summarized. This work can have a positive effect on revealing the grouting diffusion mechanism of a rock mass fracture network and guiding engineering applications.

Governing Equation of Grout Flow in a Single Rough Fracture

Based on the discrete fracture network media theory, the scholars have conducted in-depth research and obtained more mature theories on the diffusion and migration laws of grout in a single fracture. The governing equation of the grout in a single rough fracture with the assumption of cement grout as a Newtonian fluid is provided in the following.

The schematic diagram of the grout flowing in a single fracture is shown in Fig. 1. A piece of a microelement body flowing in the fracture was taken to analyze, and the effect of velocity changes was ignored. The force was maintained in balance by the radial direction of the microelement body center:

$$p\Delta y - \left(p + \frac{dp}{dx}\Delta x\right)\Delta y - \left(\tau + \frac{d\tau}{dy}\Delta y\right)\Delta x + \tau\Delta x - \rho g \sin\theta\,\Delta x\Delta y = 0 \tag{1}$$

Eq. (1) can be simplified as follows:

$$-\left(\frac{dp}{dx} + \rho g \sin\theta\right) = \frac{d\tau}{dy} \tag{2}$$

where p = grout pressure at any point in the fracture; τ = shear stress of the grout at any point; ρ = grout density; g = acceleration of gravity; and θ = fracture dip. The constitutive equation of Newtonian fluid is

$$\tau = \mu\frac{dv}{dy} \tag{3}$$

where μ = grout dynamic viscosity; and v = flow velocity of grout at any point. Eq. (4) can be obtained by combining Eqs. (2) and (3) and integrating

$$\mu\frac{dv}{dy} = -\left(\frac{dp}{dx} + \rho g \sin\theta\right)y + C_1 \tag{4}$$

the fracture aperture is assumed as b. Using the boundary condition, when $y = 0$, $(dv/dy) = 0$, into Eq. (4), it can be obtained that $C_1 = 0$.

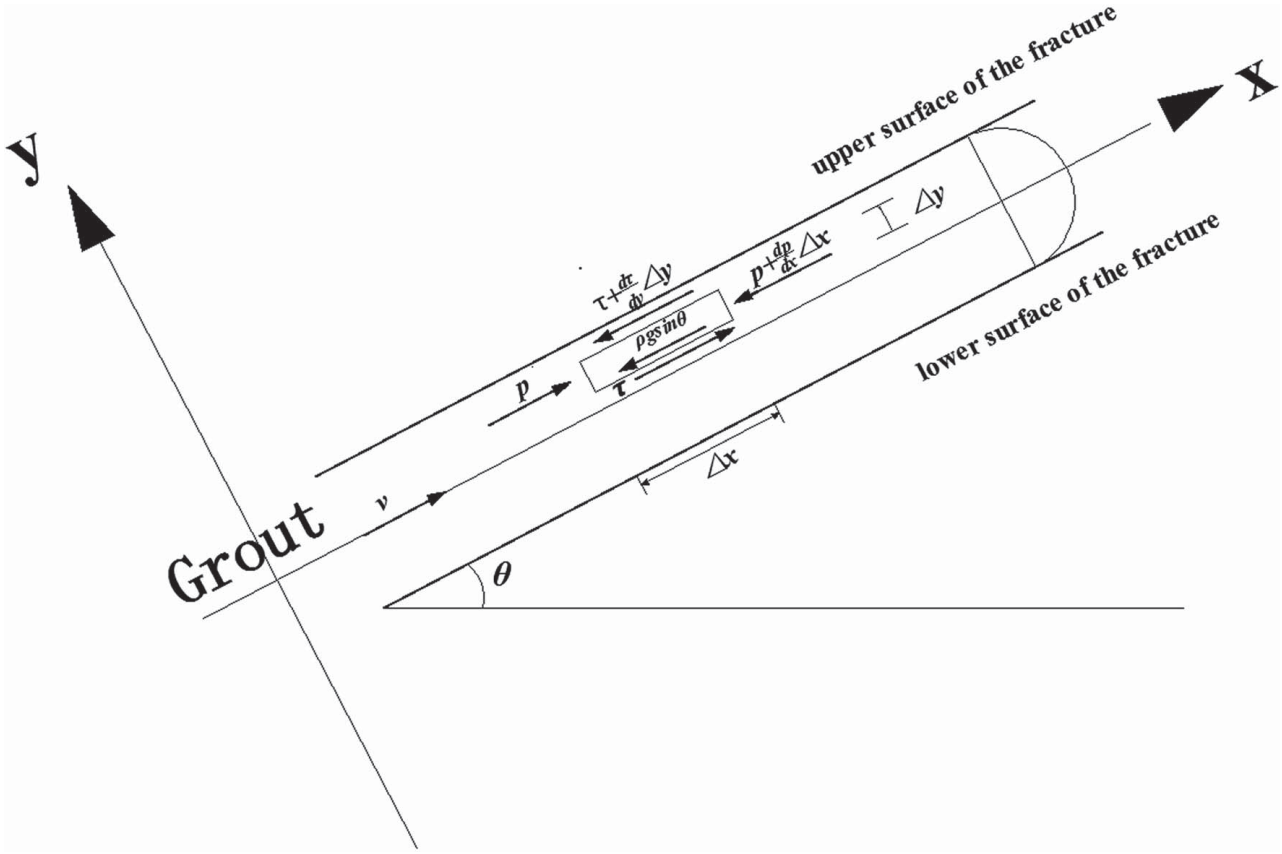

Fig. 1. Schematic diagram of the grout flowing in a single fracture.

Eq. (4) can be transformed as follows:

$$v = -\frac{1}{\mu}\left(\frac{dp}{dx} + \rho g \sin\theta\right)\frac{y^2}{2} + C_2 \tag{5}$$

Using the boundary condition, when $y = \pm(b/2)$, $v = 0$, into Eq. (5), it can be obtained that

$$C_2 = \frac{1}{\mu}\left(\frac{dp}{dx} + \rho g \sin\theta\right)\frac{b^2}{8} \tag{6}$$

Eq. (5) can be transformed to

$$v = \frac{1}{\mu}\left(\frac{dp}{dx} + \rho g \sin\theta\right)\left(\frac{b^2}{8} - \frac{y^2}{2}\right) \tag{7}$$

where the average flow velocity of the grout is

$$v_m = \frac{2\int_0^{b/2} v dy}{b} = -\frac{b^2}{12\mu} \cdot \left(\frac{dp}{dx} + \rho g \sin\theta\right) \tag{8}$$

where v_m = average velocity of the grout forehead; and x = diffusion distance of the grout at any time. When the fracture is horizontal, Eq. (8) can be transformed to

$$v_m = \frac{2\int_0^{b/2} v dy}{b} = -\frac{b^2}{12\mu} \cdot \frac{dp}{dx} \tag{9}$$

When the fracture is rough, the permeability coefficient K_g exists, and b in Eq. (9) should be changed to the equivalent hydraulic aperture. Herein, we considered the fracture aperture b as the equivalent hydraulic aperture. Then, Eq. (10) was transformed as follows:

$$v_m = \frac{2\int_0^{b/2} v\, dy}{b} = -\frac{b^2}{12\mu} \cdot K_g \cdot \frac{dp}{dx} \tag{10}$$

Eq. (10) is the analytical solution of the average velocity of the grout forehead in a single rough fracture. The flow rate q of the grout unit time can be expressed as follows:

$$q = v_m \cdot bh \tag{11}$$

Using Eq. (10) into Eq. (11), and integrating, the analytical solution of grout pressure p as a function of diffusion distance x can be obtained according to the boundary conditions of $x = 0$ m, $p = p_0$, that is,

$$p = -\frac{12q\mu}{b^3 h K_g}x + p_0 \tag{12}$$

where p_0 = grouting pressure. According to the relationship between the amount of grout injected into the fracture per unit time and the amount of grout required for the fracture diffusion distance,

$$\int_0^t q dt = b \cdot h \cdot x \tag{13}$$

then

$$x = -\frac{b^2}{12\mu} \cdot K_g \cdot \frac{dp}{dx} \cdot t \tag{14}$$

Development of a Grouting Test System in Rock Mass Fracture

To simulate the grout flow in the rock mass fracture network and visually observe the migration and diffusion process, a visualized rock mass fracture grouting test system with constant pressure was developed. The system can accurately describe the grout velocity and pressure changes at different positions in the fracture network. The system consisted of four parts: pressure supply equipment, constant-pressure pulping equipment, fracture simulation equipment, and monitoring equipment, as shown in Fig. 2. The pressure supply equipment adopted a 750-W–24-L air compressor, which provides stable and adjustable pressure for the constant-pressure pulping equipment using the pressure limited valve and branch pipe, and the provided pressure range was 0–0.8 MPa. When the grout–gas displacement test is conducted, the fracture simulation equipment can be supplied with constant gas (the gas pressure was much smaller than the grouting pressure) through the diverter valve and the pressure-limiting valve.

Constant-Pressure Pulping Equipment

The constant-pressure pulping equipment and pressure supply equipment were connected through a branch pipe to pressurize the grout. The grout tube was made of polymethyl methacrylate (PMMA) plexiglass, which can easily be observed and has certain compressive performance. The upper and lower sealing plates were made of 1,060 aluminum plates with tight sealing properties and strong pressure bearing. The protective plates were installed on three sides of a stainless steel frame to ensure the grouting test safety. After the grout was injected into the grout tube, precipitation occurred over time. Therefore, a turbine was designed at the bottom of the grout tube so that the rheological properties of the effluent grout were consistent with the design value. A pressure gauge was installed at the pulping branch to address the needs of pressure reading. The design and reality drawing are presented in Fig. 3. The constant-pressure pulping equipment

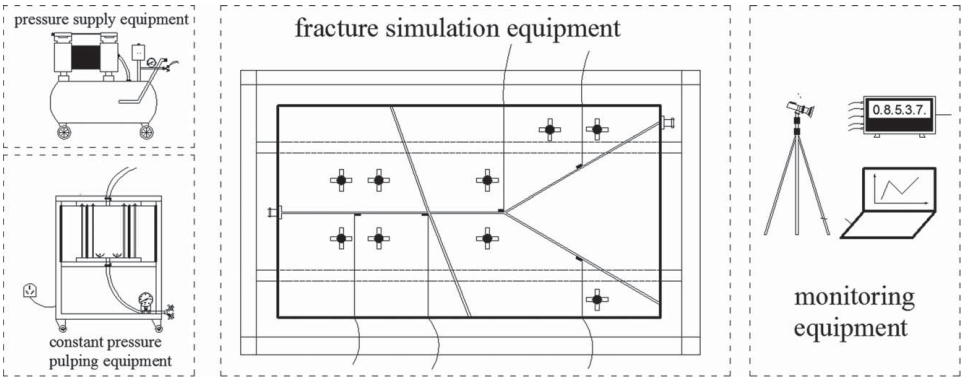

Fig. 2. Schematic diagram of the grouting test system of the rock mass fractures.

Int. J. Geomech., 2021, 21(1): 04020242

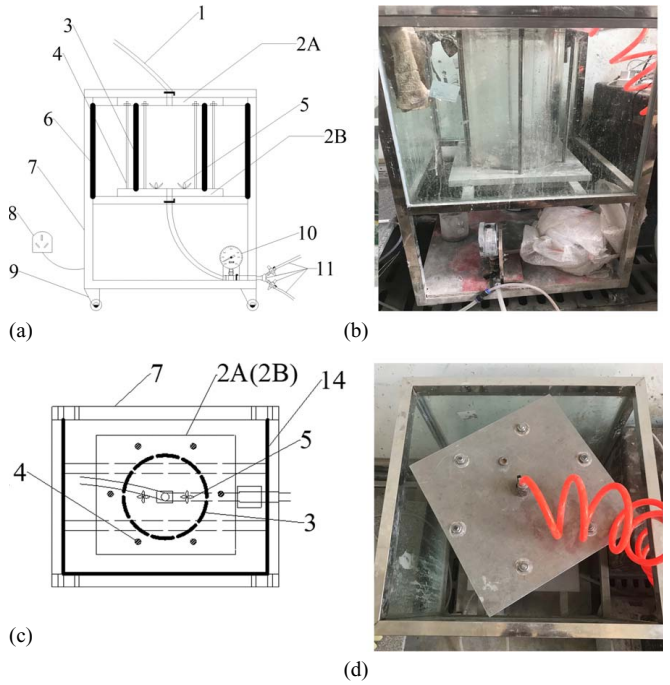

Fig. 3. Grout feed system with constant pressure: (a) front view; (b) physical map; (c) top view; and (d) physical map. 1 = branch pipe; 2A(2B) = upper(lower) sealing plate; 3 = grout tube; 4 = fastening bolts; 5 = turbines; 6 = protective plates; 7 = stainless steel frame; 8 = plug; 9 = pully; 10 = pressure gauge; and 11 = diverter valves, pressure-limiting valves.

provided constant pressure for the grouting test. In the grout–water displacement test, the fracture water with constant pressure (the water pressure was much smaller than the grouting pressure) can be provided for the rock mass fracture equipment through the diverter valve and the limiting valve.

Fracture Simulation Equipment

The fracture simulation equipment is the main platform for the grouting test in the rock mass fracture network. Two simulation platforms for a single fracture and fracture network were designed. The design and reality drawing of the fracture network equipment are displayed in Fig. 4. The marble slab was precut and prefabricated to form a fracture network consisting of bifurcation and intersection fractures, which are the basic units, as shown in Figs. 4(a and b). The pressure sensors were predisposed at the critical positions in the fracture network to real-time measure the pressure changes during the grout flow.

The upper and lower pressure plates were arranged at both ends of the fracture network, and three were fastened to a closed whole using bolts. The upper and lower pressure plates were made of PMMA plexiglass, which is convenient for observing the grout migration and diffusion process. The moving groove was designed on the upper and lower sides of the plexiglass; thus, the fracture aperture of the marble slab could be flexibly controlled according to the test design. The inlets were designed at the left and right ends of the fracture to facilitate the inflow of the grout or water/gas. The entire simulation platform was mounted on a strictly leveled stainless steel bracket, as shown in Figs. 4(c and d).

A major difficulty in the fabrication of simulation device was to keep the whole system airtight. Therefore, before the formal grouting test, tap water should be used instead of the grout for pretesting to ensure that no liquid seepage occurs during the entire flow process.

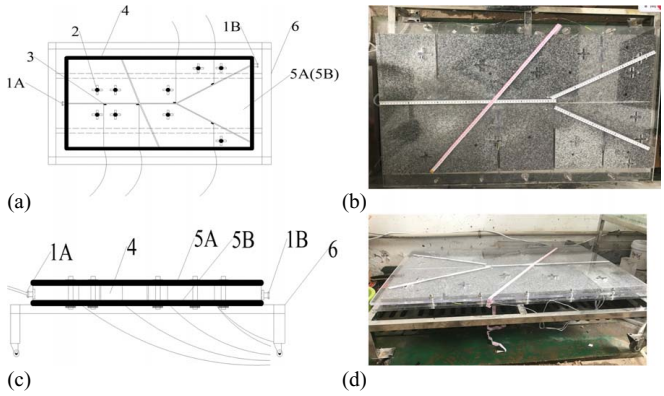

Fig. 4. Fracture simulation system: (a) front view; (b) physical map; (c) top view; and (d) physical map. 1A(1B) = grouting inlet (outlet); 2 = fastening bolts; 3 = pressure sensor; 4 = marble slab; 5A(5B) = upper (lower) plexiglass; and 6 = stainless steel frame.

Monitoring Equipment

The monitoring equipment is key to simulate the physical test of grouting in the rock mass fracture network. To quantitatively describe the flow process of the grout in the fracture network, this test primarily monitored the pressure, flow velocity, diffusion distance, and grout diffusion video. A high-speed camera was employed to capture the grout diffusion and migration video. Also, the diffusion distance and the approximate velocity of grout forehead could be calculated according to the monitoring video. The monitoring instrument and equipment are shown in Fig. 5.

The pressure sensors are placed at the critical position of the fracture to monitor the dynamic pressure during the grout diffusion process. The sensors were produced by Nanjing Danmo Technology Company, China, and the stress values were provided as follows:

$$P_i = K(F_i - F_0) \tag{15}$$

where P_i = real-time stress value of the sensor; K = calibration coefficient; F_0 = output initial strain value; and F_i = output strain value corresponding to P_i.

The dataTakerDT80G (Earth Products China Limited, Hong Kong, China) was used to read and record the measured pressure values. The interval time of reading data was set to 0.2 s, as shown in Fig. 5(b).

Technical Advantages of the Rock Mass Fracture Grouting Test System

To study the grout flow process in the rock mass fracture network, a visualized laboratory test system for grouting was designed. Compared with the existing test platforms, the test system had the following technical advantages:

1. The existing fracture grouting test systems primarily simulated the grouting process in a single fracture or orthogonal fracture network, while the engineering rock masses were all random fracture networks. The fracture simulation system of this test was based on the random fracture network, and researchers can design different fracture networks per their requirement.
2. In addition to the conventional grout flow test, the system could also simulate the fracture water or gas (i.e., air, gas) that may occur in the initial rock mass fracture. Thus, the grout–water/gas displacement mechanism in the fractured rock mass in grouting engineering was studied.
3. The as-developed test system can simulate the grout flow process under the effect of various parameters such as grouting

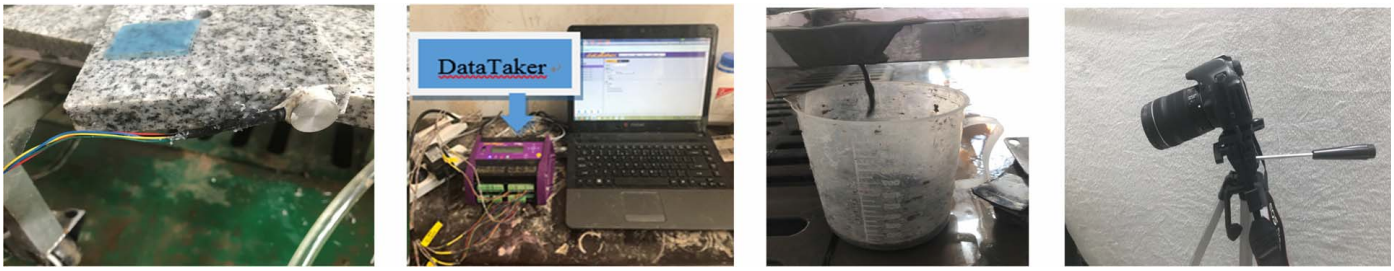

(a) (b) (c) (d)

Fig. 5. Monitoring instruments and equipment: (a) pressure sensor; (b) data acquisition instrument; (c) grout amount; and (d) high-speed camera.

(a) (b) (c) (d)

Fig. 6. Grouting test in fractures: (a) grout preparation; (b) pressure gauge rises to design pressure; (c) grouting process in a single fracture; and (d) grouting process in a fracture network.

pressure, grout characteristics (water cement ratio), fracture aperture, and fracture dig.

Grouting Simulation Test and Reliability Verification

Grouting Simulation Test

Before the grouting simulation test, the fracture aperture can be adjusted through the moving groove of the fracture platform to meet the design. Also, the pressure sensors were arranged at the key positions of the grout flowing path and the sensor leads were connected to the data acquisition instrument. The height of the tripod was adjusted so that the fracture simulation platform was completely placed in sight of the high-speed camera. An adhesive was used to seal where the lead was located, and the bolts were tightened to make the fracture a closed whole.

The cement grout was prepared according to the predetermined water–cement ratio. After the preparation, the grout was injected into the grout tube, the bolts were tightened, and the turbines were rotated by turning on the power, as shown in Fig. 6(a). The air compressor was turned on to fill the grout tube with gas, the pressure gauge was observed, and the valve was closed when the design pressure was reached, as shown in Fig. 6(b).

At the beginning of the grouting test, the valve was opened to allow the grout to flow into the fracture at a constant pressure. Simultaneously, the pressure sensors monitored the pressure changes of the grout and recorded and saved the data through the data acquisition instrument. The high-speed camera took a real-time picture of the diffusion of the grout in the fracture. After the grout stably flowed out from the exit, it reached a constant state, as shown in Figs. 6(c and d).

According to the design, the parameters such as the water–cement ratio, grouting pressure, fracture aperture, and so forth were adjusted and the aforementioned operations were repeated for the next set of tests.

Table 1. The test parameters of grouting in a single fracture

		Grouting pressure (MPa)			
Fracture aperture (mm)	w/c	0.12	0.14	0.16	0.18
1	0.7	—	—	—	—
	1.0	—	√	—	—
	1.5	—	—	—	—
	2.0	—	—	—	—
2	0.7	—	√	—	—
	1.0	√	√	√	√
	1.5	—	√	—	—
	2.0	—	√	—	—
3	0.7	—	—	—	—
	1.0	—	√	—	—
	1.5	—	—	—	—
	2.0	—	—	—	—

Note: √ = test that has been carried out under this parameter condition; — = test that has not been carried out.

Reliability Verification of the Grouting Test in a Single Fracture

To verify the reliability of the grouting system designed, the grout flow process in a single fracture was first simulated. The effects of different grouting pressures, grout water–cement ratios (w/c), and fracture apertures on the grouting diffusion process were studied. The specific test parameters are listed in Table 1. The marble plate had a thickness of 16 mm and a single fracture length of 1,000 mm. Three pressure sensors were arranged at 250, 500, and 750 mm from the grouting inlet. The high-speed camera

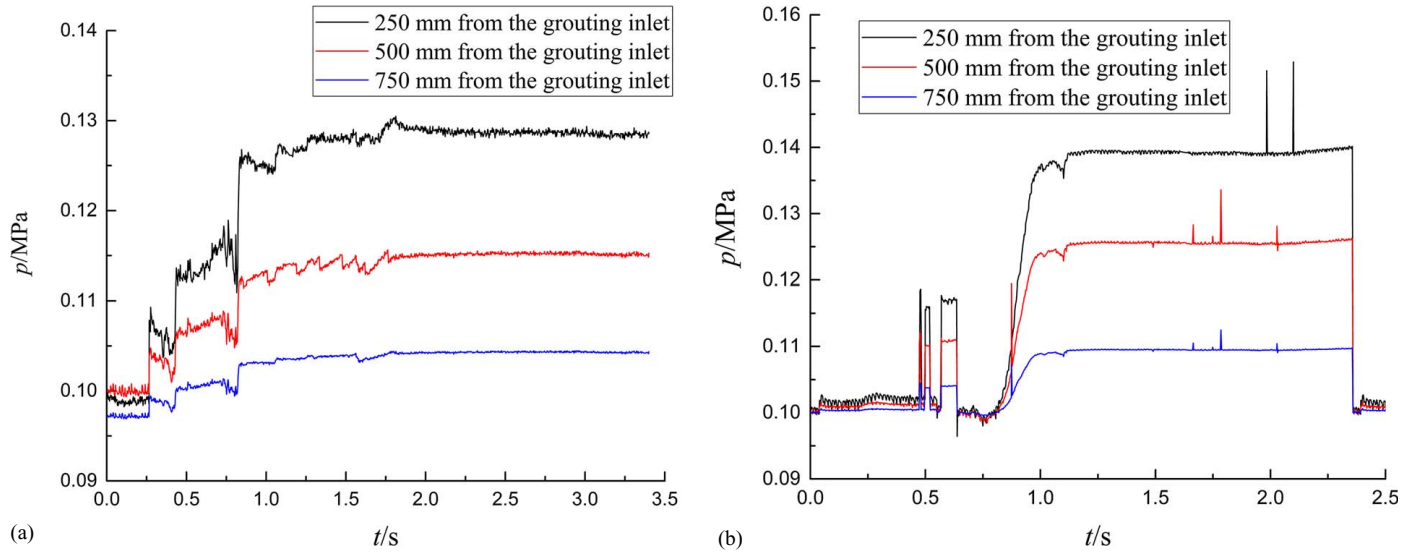

Fig. 7. Grout pressure at the measured position changes with time: (a) grouting pressure = 0.14 MPa; and (b) grouting pressure = 0.16 MPa.

Table 2. Grout diffusion distance and velocity changes with time

Time	t (s)	0	0.5	1	1.5	2	2.5
$p_0 = 0.14$ MPa	x /(m)	0	0.50	0.71	0.86	1.00	1.00
	v_m (m s^{-1})	0	1.03	0.78	0.61	0.58	0.58

captured the diffusion distance at different times, and the flow velocities of the grout forehead at different times were calculated.

Because of the length limitation of this paper, only the test results when the fracture aperture was 2 mm and grout w/c = 1:1 were presented. The grouting pressures were 0.14 and 0.16 MPa. The measured position pressure changes with time under different grouting pressures in a single fracture are shown in Fig. 7.

When the grouting pressure was 0.14 MPa, the diffusion distance and diffusion velocity at different times were calculated according to the grout flow process, as shown in Table 2.

When the diffusion distance was 0 m, the grout pressure p was 0.14 MPa, i.e., grouting pressure. When the diffusion distance was 1 m, the grout pressure was atmospheric pressure (taken as 0.1 MPa). According to the boundary conditions, a decay curve of the pressure p in the fracture with diffusion distance x can be obtained. The comparison between theoretical curves and test values is presented in Fig. 8.

As shown in Fig. 8, in a single rough fracture grouting test, the grout pressure linearly decreased with an increase in the diffusion distance. When the diffusion distance reached the end of the simulated fracture, the pressure dropped to 0.1 MPa. The test values measured by the pressure sensor were in good agreement with the theoretical curve, which proves the reliability of the designed rock mass fracture grouting test system. The system can be applied to the grouting test in a complex fracture network. Compared with the theoretical values, the test values were relatively low. The reason is that before the grout flowed out and entered the fracture channel, it passed through a small branch pipe, causing a pressure loss.

For a cement grout with the water–cement ratio of 1:1, μ is 0.019 Pa·s, b is 0.002 m, and h is 0.016 m (Liu et al. 2014). As shown in Table 2, $v_m = 0.58$ m/s at the stabilization state. Then, the permeability coefficient of the rough fracture of the marble material was $K_g = 0.83$ using Eq. (12). According to Eq. (14) and the known grout and fracture parameters, the variation curve

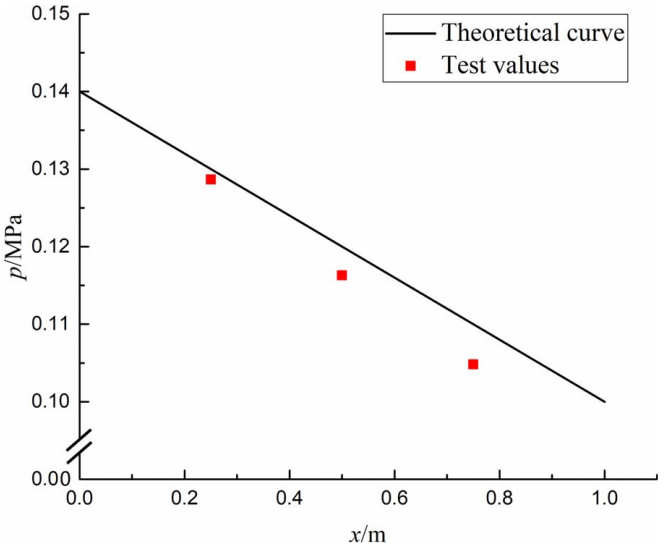

Fig. 8. Pressure changes with the diffusion distance when the grouting pressure is 0.14 MPa.

of the diffusion distance x with time t can be obtained at a grouting pressure of 0.14 MPa. The comparison between the theoretical curve and measured values is presented in Fig. 9.

As shown in Fig. 9, under constant grouting pressure, the diffusion distance increased with time and the increasing trend gradually slowed down. The diffusion distance reached a maximum value at 1 m, i.e., the end of the fracture. These measurements were in good agreement with the theoretical curves. As the grout passed through the valve, elbow, and inlet, it was subjected to resistance, resulting in pressure loss. Hence, the measured diffusion distance value was slightly smaller than the theoretical value.

Results Analysis of the Simulation Test of Grouting in a Rock Mass Fracture Network

Regarding the grout flow pattern in the rough fracture network, the test mainly investigated the effects of three parameters of the grouting pressure, fracture aperture, and grout viscosity (w/c) on the

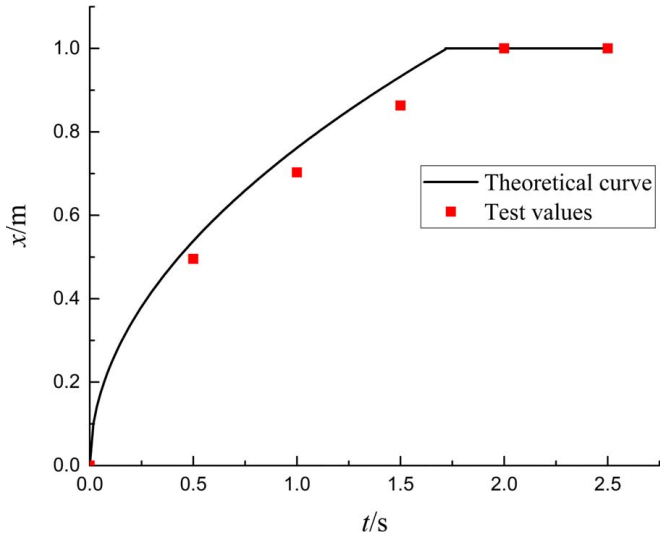

Fig. 9. Diffusion distance with the time when the grouting pressure is 0.14 MPa.

Table 3. Test parameters of grouting in the fracture network

		Grouting pressure (MPa)			
Fracture aperture	w/c	0.14	0.16	0.18	0.20
Fracture aperture = 2 mm	0.7	—	—	√	—
	1.0	√	√	√	√
	1.5	—	—	√	—
	2.0	—	—	√	—
Main aperture = 2 mm; secondary aperture = 3 mm	0.7	—	—	√	—
	1.0	—	—	√	—
	1.5	—	—	√	—
	2.0	—	—	√	—
Main aperture = 2 mm; secondary aperture = 1 mm	0.7	—	—	—	—
	1.0	—	—	√	—
	1.5	—	—	—	—
	2.0	—	—	—	—

Note: √ = test that has been carried out under this parameter condition; — = test that has not been carried out. *Main aperture* indicates the fracture aperture of main path, and *secondary aperture* indicates the fracture aperture of secondary path.

grouting process. The specific test parameters are listed in Table 3. The thickness of the marble plate material used in the test was 16 mm. The pressure distribution with time was measured by arranging seven pressure sensors at key positions. The schematic diagram of the seven sensors positions is shown in Fig. 10. The flow velocities of the grout forehead could be calculated by capturing the diffusion distance at different times using a high-speed camera.

The curves of the grout pressure at key positions in the fracture network are shown in Fig. 11. When the grouting pressure was 0.18 MPa, the w/c was 1 and the fracture aperture was 2 mm. The initial pressure of the measured points was around 0.1 MPa (atmospheric pressure). When the grout flowed through, the pressure increase in a short time and tended to stabilize after a short fluctuation near a certain value, which is the pressure value of the grout flowing through the point. In general, the grout pressure decreased as the diffusion distance increased, but the specific amplitude still needed to be analyzed in-depth. Sensors 3, 4, and 5 were located in three tributary directions of the intersection fracture, the pressure at 5 was higher than the pressures at 3 and 4. Sensors 6 and 7 were located in two tributary directions of the

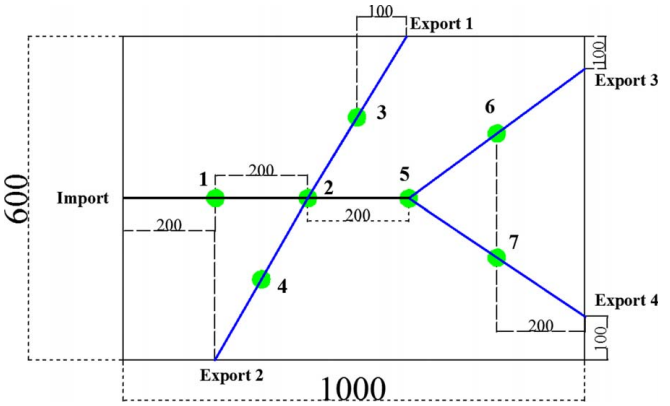

Fig. 10. Pressure sensors' positions in the fracture network. The red circle represents "Sensor 1, Sensor 2,…"; for the fracture network, the horizontal line represents the main path, and the diagonal line represents the secondary path.

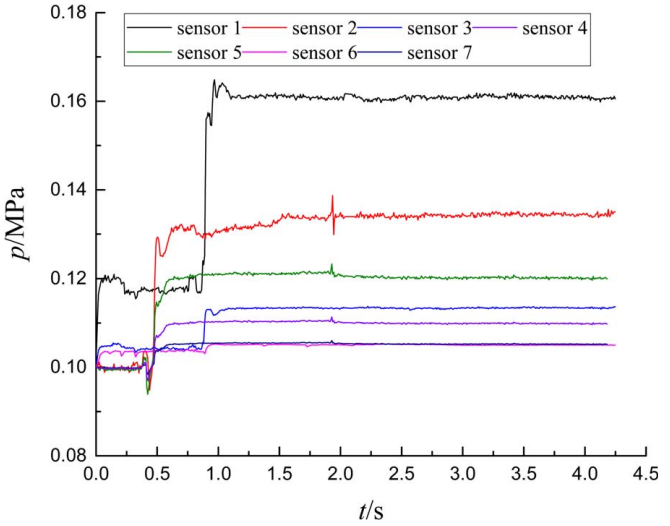

Fig. 11. Grout pressure at the key position changes with time.

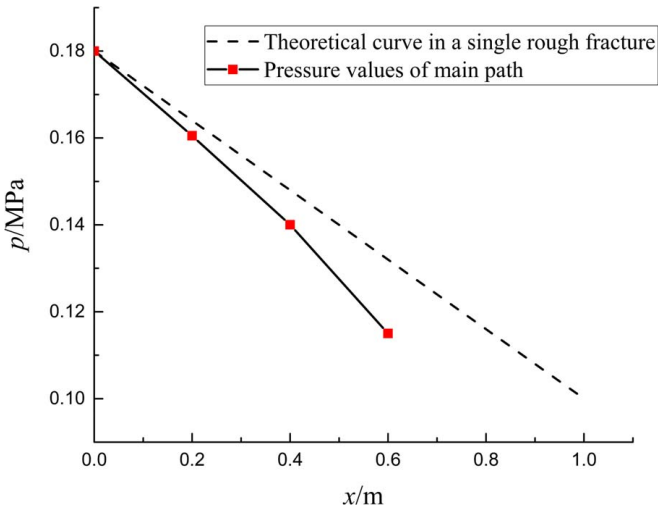

Fig. 12. Comparison of the single theoretical curve and measured values of the main path.

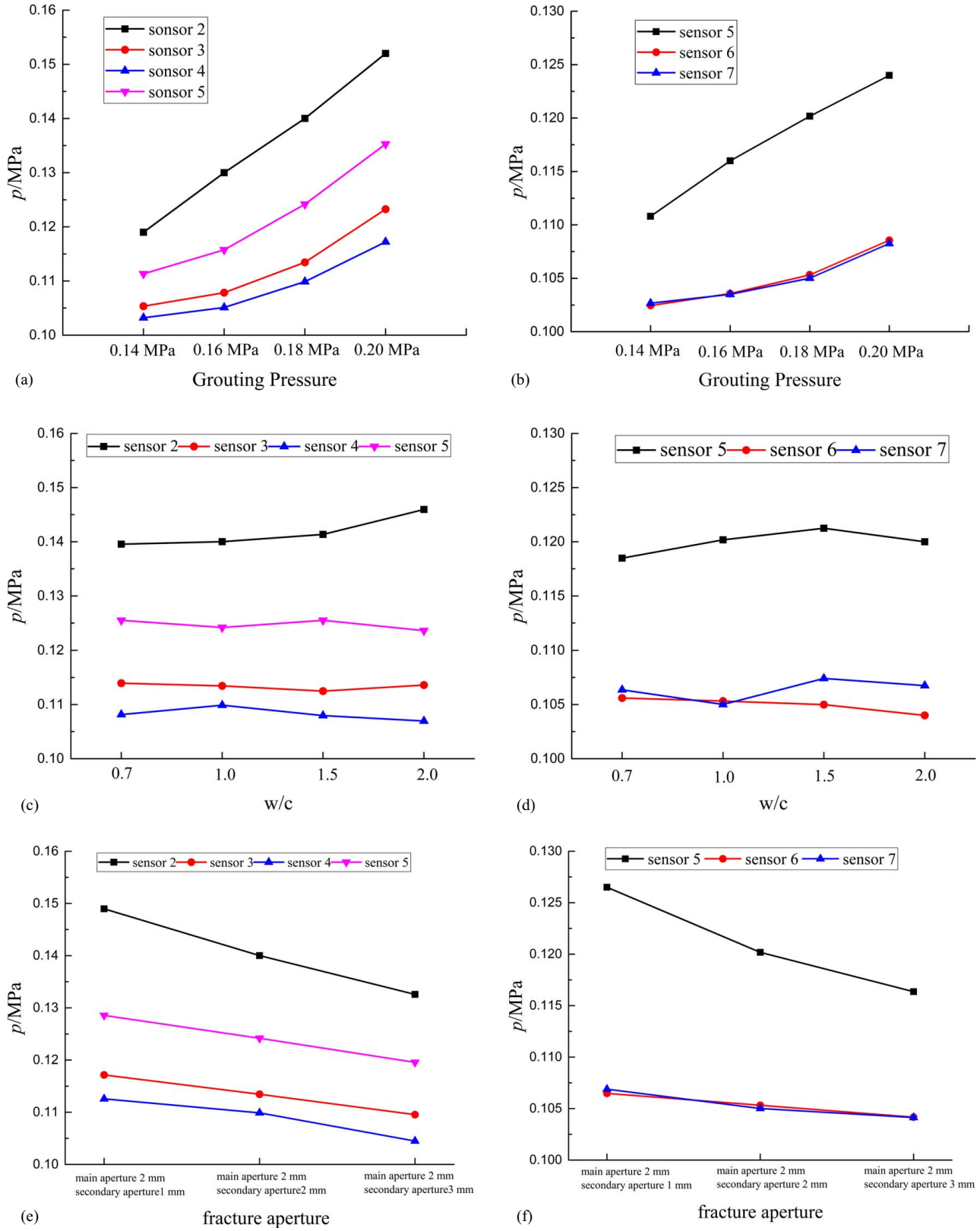

Fig. 13. Pressure changes in key positions under the influence of various parameters: (a) pressure change at the critical positions of the intersection fracture under different grouting pressures when the w/c was 1 and the fracture aperture was 2 mm; (b) pressure change at the critical positions of the bifurcation fracture under different grouting pressures when the w/c was 1 and the fracture aperture was 2 mm; (c) pressure change at the critical positions of the intersection fracture under different w/c when the fracture aperture was 2 mm and the grouting pressure was 0.18 MPa; (d) pressure change at the critical positions of the bifurcation fracture under different w/c when the fracture aperture was 2 mm and the grouting pressure was 0.18 MPa; (e) pressure change at the critical positions of the intersection fracture under different fracture apertures when the w/c was 1.0, the grouting pressure was 0.18 MPa; and (f) pressure change at the critical positions of the bifurcation fracture under different fracture apertures when the w/c was 1.0, the grouting pressure was 0.18 MPa.

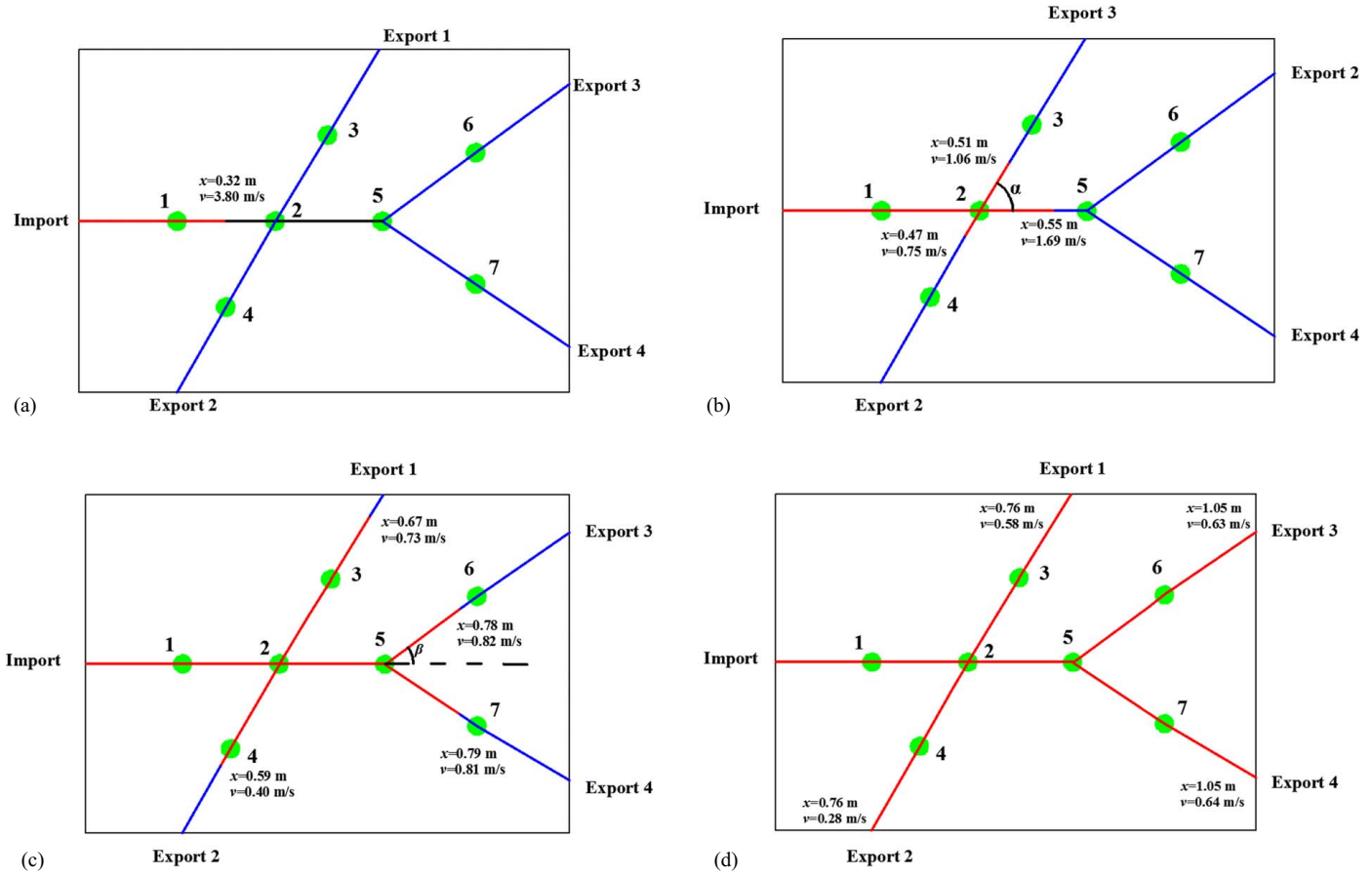

Fig. 14. Schematic diagram of grout diffusion distance and forehead velocity: (a) $t = 0.08$ s; (b) $t = 0.40$ s; (c) $t = 1.20$ s; and (d) $t = 1.85$ s.

bifurcation fracture and the pressures at Sensors 6 and 7 were basically equal. The intersection and bifurcation fractures were the basic units that formed the fracture network, and it was important to analyze the relative relationship between the internal pressures.

Fig. 12 shows the measured curve of the main path pressure in the fracture network. The theoretical pressure curve when the main path is assumed to be a single rough fracture is indicated by a dotted line. By comparison, when the grout flowed in the fracture network, the pressure loss occurred due to the existence of the branch path, and the pressure dropped rapidly. In the grouting engineering practice, a large grouting pressure is required to fill the fracture network.

Figs. 13(a and b) show the pressure change at the critical positions of the bifurcation and intersection fracture under different grouting pressures when the w/c was 1 and the fracture aperture was 2 mm. As the grouting pressure increased, the pressure at the same point increased linearly. The growth rate of the four points of the intersection fracture was between 39.9% and 55.0%, and the growth rate of the three points of the bifurcation was 9.32% and 22.0%. The effect of the decrease in the grouting pressure increased with an increase in the diffusion distance, and the impact on the main path direction was greater than that on the secondary path direction. Figs. 13(c and d) show the pressure change at the critical positions of the bifurcation and intersection fracture under different w/c values when the fracture aperture was 2 mm and the grouting pressure was 0.18 MPa. As w/c increased from 0.7 to 2.0 (i.e., the grout viscosity increased continuously), the pressures at the measured positions remained substantially unchanged, and the viscosity change could not cause the change in the internal pressure. The results from the high-speed camera suggested that as the viscosity increased, the time required for the same diffusion distance increased and the grout velocity gradually decreased. Figs. 13(e and f) display the pressure change at the critical positions of the bifurcation and intersection fracture under different fracture apertures when the w/c was 1.0, the grouting pressure was 0.18 MPa. As the fracture aperture increased, the pressure at the same point decreased linearly. For the intersection fracture, the pressure decrease at Sensor 2 was about 0.016 MPa, while the pressure decrease at Sensors 3, 4, and 5 was about 0.008 MPa. For the bifurcation fracture, the pressure decrease at Sensor 5 was about 0.010 MPa, while the pressure decrease at Sensors 6 and 7 was about 0.003 MPa. These results indicate that the initial end pressure in a fracture unit had a great influence.

The analysis of different pressure decreases at the same point is as follows. When the grout flowed in the fracture network, the import pressure was constant, which is the grouting pressure, and the export pressure was also constant, which is the atmospheric pressure, and the pressure decreased continuously with an increase in the diffusion distance. When w/c was 1 and the fracture aperture was 2 mm, as the grouting pressure increased, the pressure at the same point increased linearly. When w/c was 1.0 and the grouting pressure was 0.18 MPa, as the fracture aperture increased, the pressure drop at the same point increased, so the pressure decreased at the same point. When the fracture aperture was 2 mm and the grouting pressure was 0.18 MPa, as the w/c increased, the import and export pressures and the pressure drop at the same point were not changed, and the pressures at the measured positions remained substantially unchanged.

As shown in Figs. 13(a, c, and e), at the four points of the intersection fracture unit, the pressure at the grout inflow end was

greater than the pressure at the outflow end, and the pressures at Sensors 3, 4, and 5 were 32.7%, 21.4%, and 59.7%, respectively, of the pressure at Sensor 2. The pressure of the main path was greater than the pressure of the secondary path. When the grout flowed to the secondary path, the flow direction change caused a large pressure loss at the intersection. Also, the pressure at Sensor 3 was about 1.5 times that of the pressure at Sensor 4, which is related to the fracture angle. The fracture angle change may have quantitatively affected the pressure change. As shown in Figs. 13(b, d, and f), at the three points of the bifurcation fracture unit, the pressure at the grout inflow end was greater than the pressure at the outflow end, and the pressure at Sensors 6 and 7 were 25.7% and 27.2%, respectively, of the pressure at Sensor 5. The pressures on the two secondary paths were basically the same, which is consistent with the theory. In general, after the grout flow in the fracture was dispersed into the tributaries from the total flow, the pressure dropped significantly, and the morphology of the fracture network had an important effect on the grouting effect.

Fig. 14 shows a schematic diagram of the grout diffusion distance and the calculated velocity of grout forehead at different times captured using the high-speed camera under the conditions of the grouting pressure of 0.18 MPa, the w/c of 1.0, and the fracture aperture of 2 mm. In general, the grout diffusion distance increased over time. The diffusion abilities at four times (a–d) (i.e., the ratios of the maximum diffusion distance to the required time) were about 4.00, 1.38, 0.67, and 0.57 m/s, respectively, i.e., the grout diffusion ability gradually decreased. Compared with the velocities of the grout forehead, after the grout flowed through the intersection or bifurcation fracture, the velocity of each tributary decreased significantly compared with the velocity of the total flow. The inflow flow was the same as the outflow flow at the intersection (bifurcation) point, and the fracture aperture was the same; thus, the flow velocity into the point was equal to the sum of the flow velocity out of the point. As per the analysis of Figs. 14(b and c), the grout had a large difference in the flow velocity distribution of each tributary, which is related to the fracture angle γ. For the critical positions of the intersection fracture where Sensors 2, 3, 4, and 5 were located, the angle between tributaries 2–5 and the total flow was 0°, the angle between tributaries 2–3 and the total flow was α, the angle between tributaries 2–5 and the total flow was $180° - \alpha$. At $t = 0.40$ s, the three tributary velocities were 1.69, 1.06, and 0.75 m/s. For the critical positions of the bifurcation fracture where Sensors 5, 6, and 7 were located, the angle between the tributaries 5–6, 5–7, and the total flow was β; at $t =$ 1.20 s, the two tributaries were approximately equal. It is suspected that the distribution coefficient of each tributary is related to the fracture angle cosγ. Based on this conjecture, the quantitative relationship between the flow of each tributary and the fracture angle γ should be further studied to derive the empirical formula. When $t =$ 1.20 s, the whole grouting simulation process reached a steady state, and the parameters are shown in Fig. 14(d).

Conclusions

a. The visualized rock mass fracture constant-pressure grouting system is independently developed. The system can simulate the flow process of the random fracture network under different influence factors, such as different grouting pressures, grout characteristics, and fracture apertures, and can achieve the real-time monitoring of the pressure, flow velocity, and diffusion distance in the random fracture network.
b. Through the analysis of the grout flow in a single rough fracture, the measured values agree well with the grout flow control theory. The test system can be used to study the grout flow pattern in the fracture network.
c. The pressure at the critical positions in the fracture network increases linearly with an increase in the grouting pressure. In the laboratory testing, the growth rate at the intersection fracture is 39.9%–55.0% and the bifurcation is 9.32%–22.0%. The pressure decreases linearly with an increase in the fracture aperture. In the laboratory testing, the pressure decreases at the intersection fracture are 0.008 and 0.016 MPa and at the bifurcation fracture are 0.003 and 0.010 MPa, respectively. The pressure does not change, but the flow velocity gradually decreases with an increase in the grout viscosity.
d. After the grout passed through the intersection (bifurcation) point, the pressures and flow velocities of each tributary are significantly lower than the total flow pressure and flow velocity. Because of the different fracture angles of tributaries, the pressure decreases between the tributaries are different and the flow distribution coefficients are different.

Data Availability Statement

Some or all data, models, or code that support the findings of this study are available from the corresponding author upon reasonable request. The specific items are (1) the pressure values at the critical positions of the bifurcation and intersection fracture under different grouting pressures, fracture apertures and grout viscosity; and (2) the grout diffusion distance and the velocity of grout forehead at different times under the conditions of the grouting pressure of 0.18 MPa, the w/c of 1.0, and the fracture aperture of 2 mm.

Acknowledgments

This work was financially supported by the National Natural Science Foundation of China under Grant Nos. 51774267, 51974289, and 41807250. The anonymous reviewers are also deeply acknowledged for reviewing this article and giving their valuable comments.

Notation

The following symbols are used in this paper:

b = fracture aperture;
C_1 = constant;
C_2 = constant;
F_0 = output initial strain value;
F_i = output strain value corresponding to P_i;
g = acceleration due to gravity;
h = fracture height;
K = calibration coefficient;
K_g = permeability coefficient of the rough fracture;
P_i = real-time stress value of the sensor;
p = grout pressure at any point in the fracture;
q = low rate of the grout unit time;
t = time;
v = flow velocity of the grout at any point;
v_m = average velocity of the grout forehead;
x = diffusion distance of the grout at any time;
γ = fracture angle;
θ = fracture dip;

μ = dynamic viscosity;
ρ = grout density; and
τ = shear stress of the grout at any point.

References

Baker, C. 1974. *Comments on paper rock stabilization in rock mechanics*. New York: Muler, Springer.

Chen, C.-I., C.-K. Chen, and Y.-T. Yang. 2004. "Unsteady unidirectional flow of Bingham fluid between parallel plates with different given volume flow rate conditions." *Appl. Math. Model.* 28 (8): 697–709. https://doi.org/10.1016/j.apm.2003.12.004.

Ding, W. Q., C. Duan, Y. H. Zhu, T. C. Zhao, D. Z. Huang, and P. N. Li. 2019. "The behavior of synchronous grouting in a quasi-rectangular shield tunnel based on a large visualized model test." *Tunnelling Underground Space Technol.* 83: 409–424. https://doi.org/10.1016/j.tust.2018.10.006.

Funehag, J., and J. Thörn. 2018. "Radial penetration of cementitious grout—Laboratory verification of grout spread in a fracture model." *Tunnelling Underground Space Technol.* 72: 228–232. https://doi.org/10.1016/j.tust.2017.11.020.

Hässler, L., U. Håkansson, and H. Stille. 1992. "Computer-simulated flow of grouts in jointed rock." *Tunnelling Underground Space Technol.* 7 (4): 441–446. https://doi.org/10.1016/0886-7798(92)90074-R.

Kang, Y. S., Q. S. Liu, G. Q. Gong, and H. C. Wang. 2014. "Application of a combined support system to the weak floor reinforcement in deep underground coal mine." *Int. J. Rock Mech. Min. Sci.* 71: 143–150. https://doi.org/10.1016/j.ijrmms.2014.03.017.

Kang, Y. S., Q. S. Liu, H. L. Xi, and G. Q. Gong. 2018. "Improved compound support system for coal mine tunnels in densely faulted zones: A case study of China's Huainan coal field." *Eng. Geol.* 240: 10–20. https://doi.org/10.1016/j.enggeo.2018.04.006.

Liu, Q. S., C. B. Lu, B. Liu, and X. L. Lu. 2014. "Research on rheological behavior for cement grout considering temperature and hydration time effects." [In Chinese.] *Chin. J. Rock Mech. Eng.* 33 (S2): 3730–3740.

Minto, J., E. Maclachlan, G. Mountassir, and R. Lunn. 2016. "Rock fracture grouting with microbially induced carbonate precipitation." *Water Resour. Res.* 52 (11): 8827–8844. https://doi.org/10.1002/2016WR018884.

Xiao, F., Z. Y. Zhao, and H. M. Chen. 2017. "A simplified model for predicting grout flow in fracture channels." *Tunnelling Underground Space Technol.* 70: 11–18. https://doi.org/10.1016/j.tust.2017.06.024.

Zhang, G. L., K. Y. Zhan, Y. Gao, and W. X. Wang. 2011. "Comparative experimental investigation of chemical grouting into a fracture with flowing and static water." *Int. J. Min. Sci. Tech.* 21 (2): 201–205.

Zhang, W. J., S. C. Li, J. C. Wei, Q. S. Zhang, X. Zhang, Z. P. Li, and D. L. Xie. 2016. "Development of a 3D grouting model test system and its application." [In Chinese.] *Rock Soil Mech.* 37 (3): 902–911.